



## New MIS 19 EPICA Dome C high resolution deuterium data: Hints for a problematic preservation of climate variability at sub-millennial scale in the “oldest ice”

K. Pol <sup>a,\*</sup>, V. Masson-Delmotte <sup>a</sup>, S. Johnsen <sup>c</sup>, M. Bigler <sup>d</sup>, O. Cattani <sup>a</sup>, G. Durand <sup>b</sup>, S. Falourd <sup>a</sup>, J. Jouzel <sup>a</sup>, B. Minster <sup>a</sup>, F. Parrenin <sup>b</sup>, C. Ritz <sup>b</sup>, H.C. Steen-Larsen <sup>c</sup>, B. Stenni <sup>e</sup>

<sup>a</sup> Laboratoire des Sciences du Climat et de l'Environnement, IPSL, CEA CNRS UVSQ, CEA Saclay, L'Orme-des-Merisiers, 91191 Gif-Sur-Yvette Cedex, France

<sup>b</sup> CNRS/Université Joseph Fourier, Grenoble 1, LGGE, 54 Rue Molière, 38410 Saint Martin d'Hères Cedex, France

<sup>c</sup> Centre for Ice and Climate, Niels Bohr Institute, University of Copenhagen, Juliane Maries Vej 30, DK-2100 Copenhagen, Denmark

<sup>d</sup> Climate and Environmental Physics, Physics Institute, and Oeschger Centre for Climate Change Research, University of Bern, Sidlerstrasse 5, 3012 Bern, Switzerland

<sup>e</sup> Università di Trieste, Dipartimento di Scienze Geologiche, Ambientali e Marine, Via E. Weiss 2, 34127 Trieste, Italy

### ARTICLE INFO

#### Article history:

Received 15 December 2009

Received in revised form 6 July 2010

Accepted 15 July 2010

Available online 21 August 2010

Editor: P. DeMenocal

#### Keywords:

water stable isotopes

ice cores

Antarctica

isotopic diffusion

### ABSTRACT

Marine Isotope Stage 19 (MIS 19) is the oldest interglacial period archived in the EPICA Dome C ice core (~780 ky BP) and the closest “orbital analogue” to the Holocene – albeit with a different obliquity amplitude and phase with precession. New detailed deuterium measurements have been conducted with a depth resolution of 11 cm (corresponding time resolution of ~130 years). They confirm our earlier low resolution profile (55 cm), showing a relatively smooth shape over the MIS 20 to MIS 18 time period with a lack of sub-millennial climate variability, first thought to be due to this low resolution. The MIS 19 high resolution profile actually reveals a strong isotopic diffusion process leading to a diffusion length of at least ~40 cm erasing sub-millennial climate variability. We suggest that this diffusion is caused by water-veins associated with large ice crystals at temperatures above  $-10^{\circ}\text{C}$ , temperature conditions in which the MIS 19 ice has spent more than 200 ky. This result has implications for the selection of the future “oldest ice” drilling site.

© 2010 Elsevier B.V. All rights reserved.

### 1. Introduction

The EPICA Dome C ice core providing more than 800 thousands of years (ky) of climate variability is the longest available climatic record obtained from ice cores. Thanks to different proxies such as stable water isotopes (Jouzel et al., 2007), aerosols (Lambert et al., 2008; Wolff et al., 2010a),  $\text{CH}_4$  (Loulergue et al., 2008; Spahni et al., 2005) or  $\text{CO}_2$  (Lüthi et al., 2008; Siengenthaler et al., 2005), local, regional and global variations of climate and environment have been characterized over eight glacial–interglacial cycles (Fig. 1). If long term climate variability is considered to be driven by variations of incoming insolation due to slow changes of orbital parameters (Berger and Loutre, 1991; Laskar et al., 1993), the precise role of seasonal and latitudinal insolation distribution remains disputed. The climate system response involves threshold effects and internal feedbacks, making the understanding of the Earth climate complex (Paillard, 1998).

Interglacial periods offer the possibility to compare the climate system response under different orbital configurations and without the major influence of northern hemisphere glacial ice sheets. Thanks to EPICA Dome C ice core strong differences have been revealed between

the nine past and current interglacial periods regarding their duration, trend or intensity (Figs. 1 and 2) (EPICA-community-members, 2004; Jouzel et al., 2007; Masson-Delmotte et al., 2010). The current interglacial period has been compared to past interglacials with a specific focus on Marine Isotope Stage (MIS) 5 and 11 (Loutre and Berger, 2003; Loutre, 2003; Masson-Delmotte et al., 2006; Ruddimann, 2005), with implications for the future long term influence of Earth's orbit and the timing of the next Ice Age.

In this context, the following study focuses on the oldest interglacial archived in the EPICA Dome C (EDC) ice core: MIS 19, occurring around 780 thousands of years (ky) before present (B.P.). The full sequence of events, from the end of the previous glacial period (MIS 20) to the beginning of the following one (MIS 18), is detected between depths of 3147 and 3190 m. Corresponding ages range between ~749 and ~801 ky with an absolute uncertainty of 6 ky ( $2\sigma$ ) (Fig. 3) as given by the current EDC3 chronology (Parrenin et al., 2007a). This dating is relatively well constrained for MIS 19, thanks to the Matuyama–Brunhes geomagnetic reversal identification from Beryllium 10 measurements (Dreyfus et al., 2008; Raisbeck et al., 2006). The integrity of the climate records in EDC ice is confirmed down to ~801 ky (Jouzel et al., 2007), despite indications of ice flow perturbation in the bottom part of the core (Dreyfus et al., 2007).

MIS 19 is interesting for two reasons: (i) it occurred during an orbital configuration quite similar to the present one; and (ii) the EPICA Dome C low resolution proxy records exhibit comparable

\* Corresponding author. Tel.: +33 1 69 08 27 02; fax: +33 1 69 08 77 16.

E-mail address: [katy.pol@lscce.ipsl.fr](mailto:katy.pol@lscce.ipsl.fr) (K. Pol).

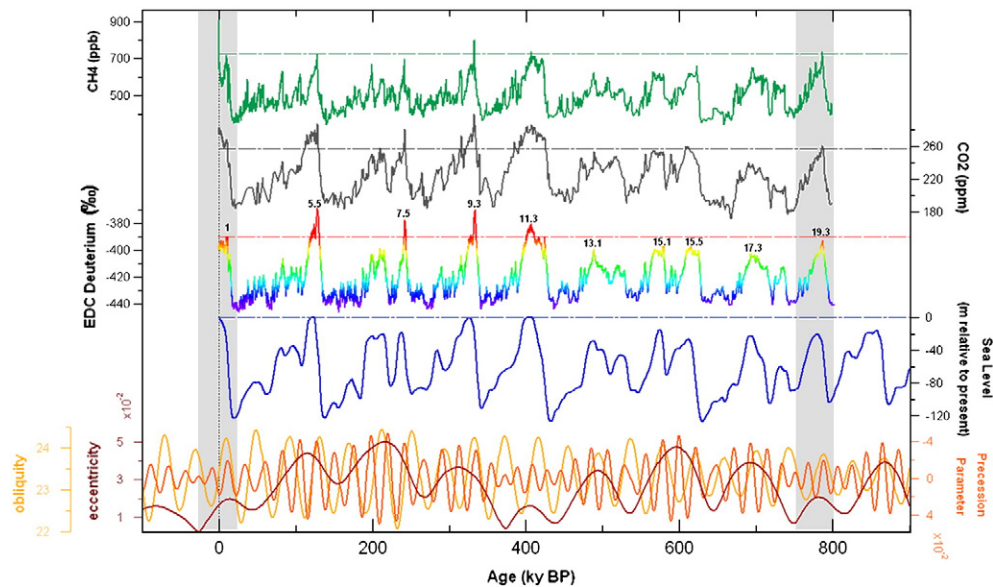


**Fig. 1.** Insolation forcing and climate variability over 800 thousands of years before present (B.P. = before 1950) recorded in different proxies. From top to bottom: EDC CH<sub>4</sub> concentrations (ppb, green) (Louergue et al., 2008; Spahni et al., 2005); CO<sub>2</sub> concentrations from Vostok and EDC ice cores (ppm, grey) (Lüthi et al., 2008; Siengenthaler et al., 2005); EDC low resolution  $\delta$ D signal (‰) (rainbow colours highlighting glacial periods, dark blue, and interglacial periods, yellow-red); reconstructed sea levels (in m relative to present-day, blue) (Bintanja et al., 2005). Changes in orbital parameters are displayed in the bottom panel (Berger and Loutre, 1991): obliquity (°, yellow), inverted precession parameter (orange), eccentricity (dark red). The two periods of interest here, from the past 20 ky to the next 10 ky and the MIS 20 to 18, are highlighted by grey-shaded areas. Horizontal lines represent the maximum pre-industrial Holocene levels. All the Marine Isotopic Stages corresponding to the Antarctic interglacials recorded in the EDC core are labelled following Jouzel et al. (2007).

magnitudes for MIS 19 and the Holocene (Figs. 1 and 2). Section 2 is thus dedicated to a detailed comparison of orbital contexts and EPICA records for these two periods.

During the glacial inception from MIS 19 to MIS 18, the low resolution EPICA Dome C water stable isotope record (Jouzel et al., 2007) has revealed millennial variability principally marked by the occurrence of three consecutive warm events (hereafter called Antarctic Isotope Maxima – AIM, following EPICA-community-members, 2006, and noted A, B, C on Fig. 2). These AIM events were also identified in the CH<sub>4</sub> and CO<sub>2</sub> signals (Louergue et al., 2008; Lüthi et al., 2008). To improve the temporal resolution and to document the sub-millennial climate variability during MIS 19, we have conducted new high resolution measurements of water stable isotope ratios ( $\delta$ D of HDO molecules, hereafter called deuterium) on the EDC ice core fine cuts (Section 3). This new sampling, allowing to increase the temporal resolution from ~650 years (low resolution published data) to ~130 years, confirms the robustness of the previous low resolution isotopic signal (Section 4.1) but reveals at the same time a strong smoothing of the deuterium signal (Section 4.2), which erases potential new information on climate variability. This result leads to an analysis of the isotopic diffusion in ice, a process commonly studied for its implication in the impairment of climatic signals (Section 4.3). Section 4.4 is then dedicated to the comparison between modelled and data-derived diffusion calculation. This comparison suggests that the deepest EDC ice is affected by physical processes that alter the preservation of the full stable isotope variability. We finally investigate the possible mechanisms at play.

## 2. Comparison of MIS 19 and Holocene orbital contexts and EPICA proxy records

We compare the orbital configurations around MIS 19 and of the current interglacial, both characterized by a low eccentricity and therefore small variations of the precession parameter (Fig. 1). By aligning the respective early interglacial maxima of MIS 1 (~11 ky BP) and MIS 19 (~787 ky BP, according to the EDC3 chronology, Parrenin et al., 2007a), Fig. 2 enables a more detailed comparison of orbital

contexts over a 50 ky interval (panels e and f). The EDC3 dating method (Parrenin et al., 2007b) is constructed independently from the  $\delta$ D orbital signal (it uses information from the  $\delta^{18}$ O of the di-oxygen in air Dreyfus et al., 2007).

This alignment shows that the interglacial optima occur during eccentricity maxima, and with exactly comparable values of the precession parameter. Because the EDC  $\delta$ D record exhibits a strong obliquity component, it was argued that the amplitude modulation of obliquity could explain interglacial intensities (Jouzel et al., 2007, Supplementary material; Masson-Delmotte et al., 2006). Differences in the orbital contexts indeed appear regarding the obliquity amplitude and its phase with the precession parameter. Due to its long term modulation (Berger and Loutre, 1991), recent obliquity variations have stronger amplitude than during MIS 19. The maximum of obliquity occurs perfectly in phase with the precession parameter minimum at 787.5 ky BP for MIS 19, while it lags by 2.5 ky the same precession parameter minimum occurring at 11.5 ky BP in the early Holocene (Table 1). In the future, the eccentricity will decrease much more strongly than at the end of MIS 19, damping the precession parameter fluctuations, but obliquity variations will keep larger amplitude than for MIS 19. This comparison shows the lack of a perfect orbital analogue but highlights that, as seen on Fig. 1, the orbital context of MIS 19 is closer to the present one than during MIS 5e or 11.

We now compare the climate evolution for MIS 19 and the Holocene in EDC3 proxy records. After a continuous warming during the transition MIS 20 to MIS 19, the deuterium signal reaches a maximum value at ~787 ky (Fig. 2b). This pattern differs from the last termination, marked by the Antarctic Cold Reversal (Jouzel et al., 1995; Jouzel et al., 2001) (Fig. 2a). When converted into temperature, after correction of sea-water isotopic and elevation changes (Jouzel et al., 2007), MIS 19 is the warmest interglacial period recorded in the EDC temperature reconstruction between 800 and 400 ky. Its peak warmth is ~0.5 °C colder than the present-day and 2 °C colder than the early Holocene optimum. Temperature reconstructions can be affected by changes in EDC elevation, with a dry adiabatic lapse-rate of ~10 °C per 1000 meters (m). However ice sheet models (Parrenin et al., 2007b; Pollard and

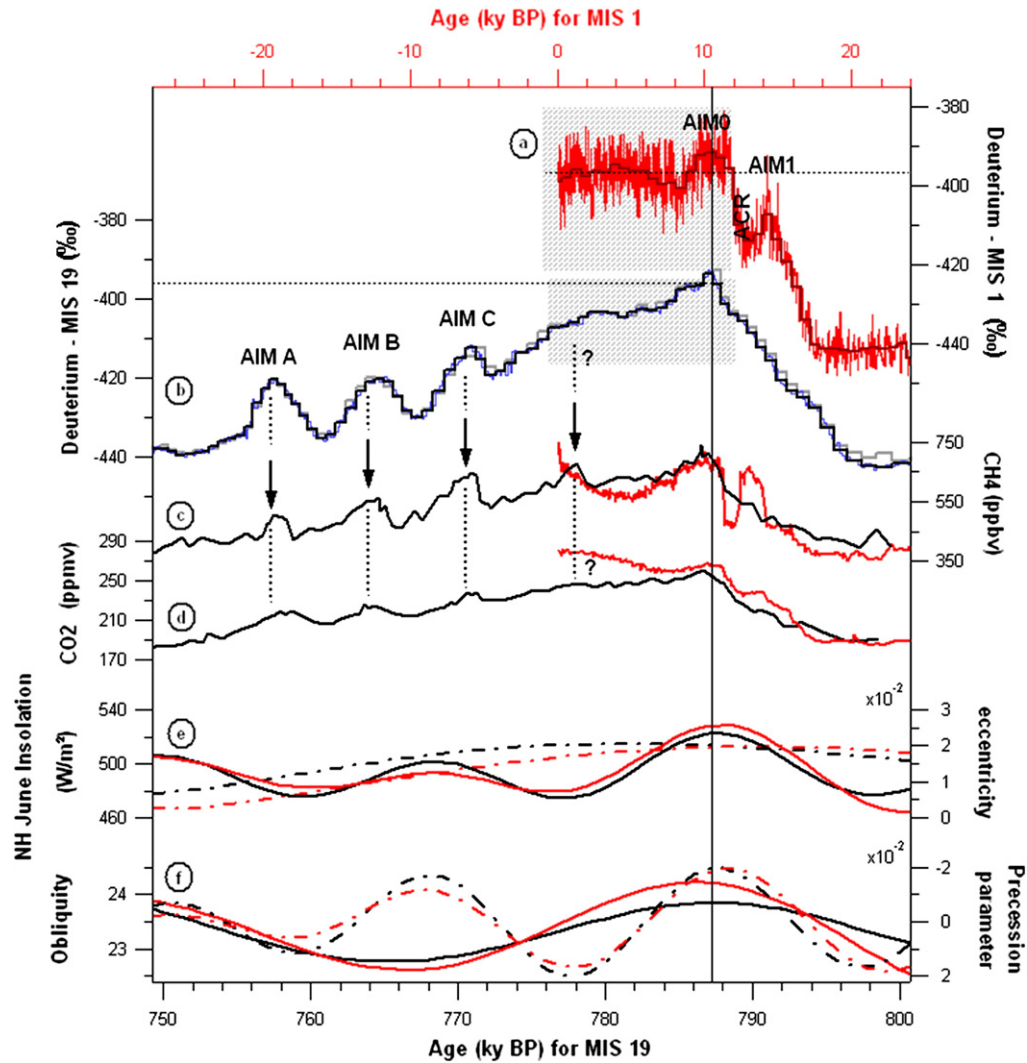


**Fig. 2.** Detailed comparison of 50 ky intervals centred on Holocene (red) and MIS 19 (black). The arbitrary alignment of the two periods is marked by the vertical black line. From top to bottom: a)  $\delta D$  (‰) of Holocene low resolution samples (red) and the corresponding 650 years averaged signal (dark red); b) MIS 19  $\delta D$  (‰) data are displayed for low resolution samples (grey, directly comparable to the dark red curve of panel a), high resolution samples (blue) and the mean signal obtained by an average of five high resolution samples (black). In panels a) and b) the thin dashed horizontal lines correspond to the present-day (last millennium average)  $\delta D$  levels; the grey shadow areas delimitate the 12 ky intervals for interglacial spectral analysis displayed in Fig. 4; c)  $CH_4$  concentrations (Loulergue et al., 2008; Spahni et al., 2005); d)  $CO_2$  concentrations (Monnin et al., 2001; Lüthi et al., 2008; Siengenthaler et al., 2005); e) eccentricity (dashed, right axis) and North Hemispheric June 21st insolation (solid, left axis); f) precession parameter (dashed, right axis), reported on inverted axis to evolve in phase with the NH insolation, and finally obliquity ( $^\circ$ , solid, left axis).

DeConto, 2009) suggest too small elevation changes ( $\sim 30$  m) between MIS 19 and Holocene to have significant impacts on temperature estimates. The difference between MIS 19 and Holocene maximal temperatures is thus robust and contrasts with the significant differences observed in reconstructions of past sea level. Based on marine data, MIS 19 sea level is estimated  $\sim 20$  m below present-day (Bintanja et al., 2005). Greenhouse gases also exhibit atmospheric concentrations comparable for MIS 19 and the pre-industrial Holocene (Fig. 2c and d).  $CH_4$  levels reach around 700 ppb both in early Holocene and at MIS 19 maximum, albeit with different patterns. During the last deglaciation, the methane curve is interrupted by the Younger Dryas event, followed by an early Holocene optimum, a mid-Holocene minimum and a progressive increase during last millennia. Prior to MIS 19 optimum,  $CH_4$  shows a continuous rise. After the MIS 19 optimum, it shows a stable plateau, followed by a decreasing trend punctuated by four maxima, the last three being the  $CH_4$  counterparts of the AIM A, B, C as noted in Lüthi et al. (2008).  $CO_2$  values reach around 260 ppm at the early Holocene and during MIS 19 maximum.  $CO_2$  increases slightly during the course of Holocene, while it is marked by a

progressive decrease for MIS 19 after the early peak value, with the occurrence of the three  $CO_2$  counterparts of AIM A, B, and C.

### 3. Data

The insert in Fig. 3 shows the cutting scheme for the EPICA Dome C ice core. The  $\sim 3260$  m of the core is continuously cut in two different ways for the water isotopes measurements: the first type of samples called “bag” samples (hereafter low resolution LR) is cut every 55 cm along the core with 9 mm square sides; the second type of samples called “fine” samples (hereafter high resolution HR) corresponds to 11 cm long paved pieces. The analysis of these HR samples therefore improves both the depth resolution and the temporal resolution by a factor of 5.

Thanks to deuterium measurements conducted on 5800 LR samples all along the  $\sim 3260$  m of the EDC ice core, a continuous but low resolution profile is available and has been used to estimate past EDC temperature (Jouzel et al., 2007). Due to ice thinning, the temporal resolution of the LR samples is strongly decreasing with

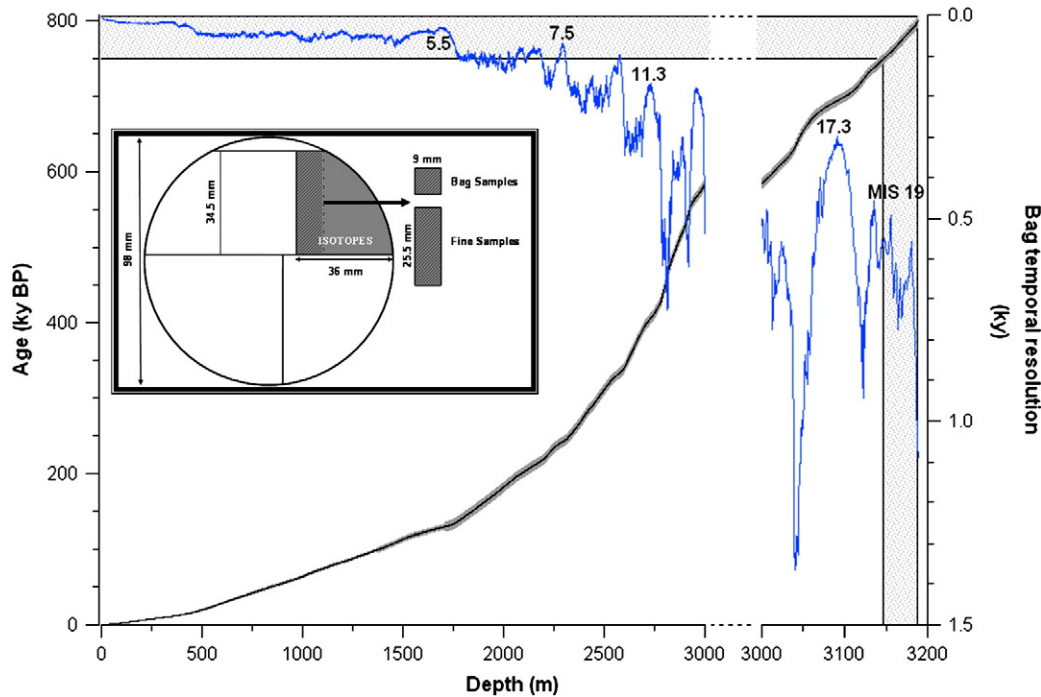


**Fig. 3.** Cutting scheme for EDC ice core samples and EDC3 age model (ky as a function of depth in m, left axis) in black (Parrenin et al., 2007b). The temporal resolution of low resolution samples is displayed in blue (number of years contained in 55 cm of ice, right axis). Due to enhanced interglacial accumulation, interglacial periods appear as intervals of higher resolution (MIS 5.5, 7.5, 9.3, 17.3 and the entire MIS 19 are labelled). The published age scale uncertainty is displayed as a grey shadow. The depth scale is divided in two parts: one from 0 to 3000 m, the second one from 3000 to 3200 m to zoom on MIS 19 corresponding depth. The age-depth characteristic of MIS 19 is highlighted by the grey-shaded area.

depth. It is also lower during glacial periods characterized by a lower accumulation. Thus while each LR sample contains in average 20 years of accumulation for the Holocene, it represents up to ~650 years for MIS 19 using the EDC3 chronology (Fig. 3). Therefore, there is a strong added value to measure the HR data for MIS 19, which are expected to enhance the temporal resolution up to ~130 years and improve the description of centennial to millennial variability.

As already mentioned, the sequence of events of interest here, covering the previous glacial period (MIS 20), MIS 19 and the beginning of the following MIS 18, extends between depths of 3190 and 3147 m. 395 HR samples have been measured in deuterium over this depth interval. Based on uranium reduction of water to H<sub>2</sub> gas (see Vaughn et al., 1998, for the description of the method), the method of measurement is the same as the one used in the past for the LR samples (Jouzel et al., 2007). The analytical accuracy is on average  $\pm 0.5\%$  at  $1\sigma$ . Fig. 2b displays the initial LR data (grey), the new HR data (blue), and a calculated mean signal (average of five HR data, black), used to compare the coherency between the past and the new data. The LR signal is statically less accurate ( $0.5\%$  at  $1\sigma$ ) than the averaged signal ( $\pm 0.23\%$  at  $1\sigma$ ) which benefits from an experimental noise reduced by a factor of  $\sqrt{5}$  (thanks to the 5 measurements used for the establishment of the HR profile instead of one for the LR profile, over the same 55 cm depth interval).

**Table 1**

Values of the three orbital parameters at 788 ky BP and 12 ky BP for respectively MIS 19 and Holocene, according to the phasing presented in Fig. 1b. The maximum Holocene obliquity value occurs at 9 ky BP (2.5 ky after the precession parameter minimum), in contrast with the perfect phasing observed for MIS 19 between the precession and obliquity extrema at 787.5 ky BP.

	Eccentricity	Precession parameter	Obliquity (°)	Lag between precession min and obliquity max (ky)
788 ky BP	0.019846	-0.019776	23.851	0
12 ky BP	0.019613	-0.019440	24.159	2.5

We also consider EDC chemistry data measured by Continuous Flow Analysis (CFA), with a high depth resolution of 1 to 1.5 cm, previously published for the Holocene and MIS 5.5 (Bigler et al., 2010) and made available here for MIS 19. Concentrations of calcium, sodium and ammonium are expected to reflect variations in aerosol emissions, transport and deposition in relation to continental dust, sea salt and marine productivity respectively (Wolff et al., 2010a). Fig. 4 displays the comparison between Holocene and MIS 19 data, both filtered at centennial resolution to allow a direct comparison of variability, as the measuring resolution is just sufficient enough to capture centennial resolution in MIS 19.

## 4. Results and discussion

### 4.1. Results description

The high resolution data (Fig. 2b, blue) show a good agreement with the low resolution data (grey). They confirm the regular deuterium increase along the transition MIS 20 to MIS 19, the shape of MIS 19 optimum, and the occurrence of three consecutive Antarctic Isotopic Maxima (noted A, B and C) during the transition to MIS 18. The “calculated” signal (black) compared to low resolution data (grey) confirms the quality of measurements along MIS 19 and 18, with a satisfying correspondence between the two signals. In a few cases (MIS 20, MIS 19 peak warmth and AIM C) the grey curve appears slightly higher than the black one. According to the respective accuracy of our two comparable signals, 50% of the measurements overlap perfectly during the full sequence of events. This value is improved up to 70% by keeping away the transition MIS 20 to MIS 19 and AIM C, characterized by low resolution values systematically shifted by +1.7‰ in average.

The differences between the two datasets (LR versus average of HR data) can arise from: (i) analytical noise; (ii) small isotopic composition differences within two different sections of ice core (see the cutting scheme of Fig. 3 for the target sections used for LR and HR sampling); and (iii) the difficulties for the sampling procedure in the deepest warm

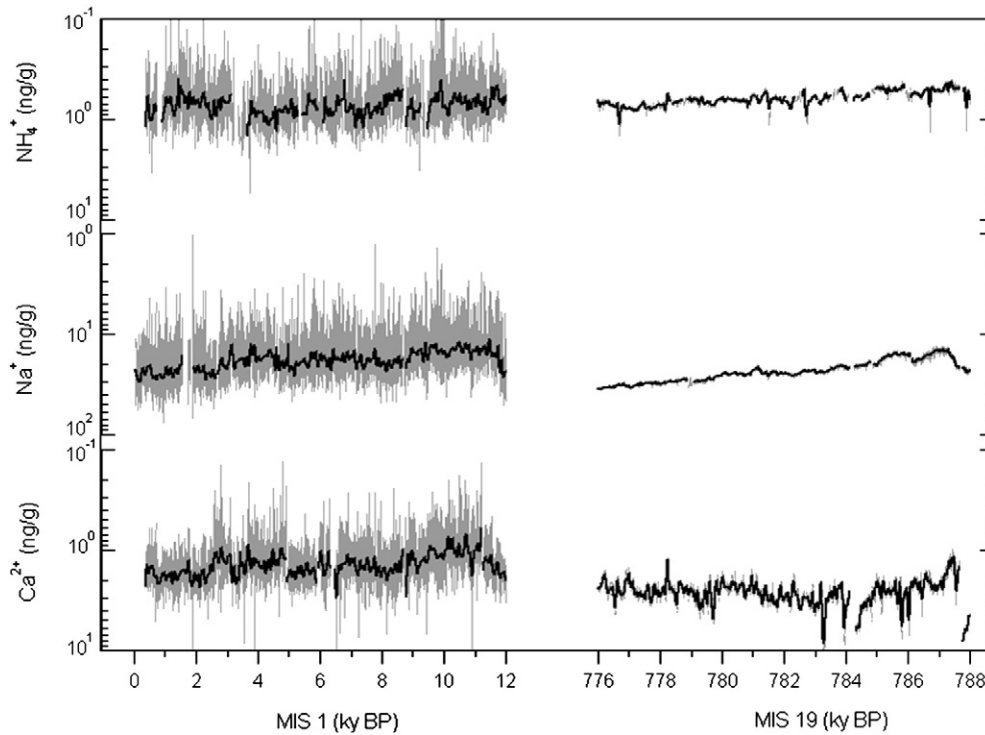


**Fig. 4.** EDC high resolution chemistry data (1 mm) displayed from 0 to 12 ky BP for Holocene (left) and from 776 to 788 ky BP for MIS 19 (right). From top to bottom: ammonium  $\text{NH}_4^+$  (ng/g), sodium  $\text{Na}^+$  (ng/g) and calcium  $\text{Ca}^{2+}$  (ng/g) concentrations are represented on reversed logarithmic scale. Formal annual means (grey) and filtered centennial resolution data (black).

ice. At this depth, the presence of cracked ice and the trimmed edges of the core caused by the alcohol used as drilling fluid may have altered the integrity of the samples. For the same isotopic measurement of 55 cm of the core, 5 samples are necessary to the reconstruction of the averaged HR signal against one in the LR signal. Thus, if a loss of ice material is involved, it may have impacted in a larger proportion the HR signal, which undergoes repeated cutting processing, than the LR signal.

Beyond confirming low resolution data, the high resolution data do not deliver significant additional sub-millennial variability information as expected from higher temporal resolution. This result contrasts with the sub-millennial variability clearly observed for the Holocene on EDC stable isotope data (Fig. 2a, comparison between red and dark red curves) and is persistent over recent interglacials (MIS 5.5 and MIS 11 unpublished high resolution deuterium data, not shown).

The persistence of a sub-millennial climate variability during MIS 19 is also independently confirmed by the high resolution EDC chemistry data showing similar level of variability during Holocene, MIS 5.5 (not shown here, Bigler et al., 2010) and MIS19 for calcium concentration, a proxy of continental dust (Fig. 4). By contrast, ammonium and sodium records show almost no more sub-millennial variability for MIS 19. The change in variability can be quantified by the calculation of variation coefficients based on de-trended logarithmic centennial resolution concentration data, from relatively stable 5000 year (noted y hereafter) intervals within each interglacial. For calcium, the variation coefficient shows similar high values for the Holocene (11.7%) and MIS 19 (15.7%), while it is a factor of two smaller for sodium (from 8 to 3.6%) and ammonium (from 11.2 to 5.8%).

#### 4.2. Spectral analysis of variability

To illustrate the loss of variability in the stable isotope data, we calculate the power spectrum for our two periods during each warm phase (from 12 ky BP to present-day for Holocene and from 788 ky BP to 776 ky BP for MIS19) with different time resolutions (Fig. 5). For MIS 19, we compare the power spectrum obtained from low resolution

data (with a temporal resolution of 650 y) to the one derived from high resolution data with a regular re-sampling of 150y. These two spectra are confronted to those performed for the Holocene, using data re-sampled every 650 and 150 y for an exact comparison.

MIS 19 power spectra first confirm the interest of looking at high resolution data for studying climatic variability. While the ~650 y re-sampled data hardly show millennial variability for both MIS 19 (only long term trends appear significant) and Holocene, the 150 y re-sampled data firstly confirm the periodicities already present in the 650 y power spectrum and make higher frequencies significant (two more peaks for MIS 19 ~2.55 ky and ~1.65 ky, and trend for Holocene). But the strong decrease of the MIS 19 spectral amplitude with frequency contrasts with the constant level of the Holocene one (both with 20 and 150 y re-sampled data). The MIS 19 spectrum based on the 150 y re-sampled data reveals a loss of signal for periodicities shorter than 1600 y, whereas the Holocene data clearly show centennial periodicities at the same resolution.

Based on the entire power spectrum of Holocene (showed in Fig. 5 and already studied by Masson et al., 2000; Masson-Delmotte et al., 2004; Yiou et al., 1997) and on the sub-millennial deuterium variability observed during previous interglacials (MIS 5.5, 9 and 11 data offering centennial resolution, not shown), our working hypothesis is that multi-decadal to multi-centennial variability must indeed be a common feature of all interglacials. This is also supported by the variability preserved in the MIS 19 calcium data (Fig. 4). Such variability for MIS 19 is thus thought to have been erased in the stable isotope, ammonium and sodium data and the following sections are dedicated to the understanding of the particular diffusion processes at play, appearing only in the deepest part of the EDC core.

#### 4.3. Isotopic diffusion modelling

Isotopic diffusion is the main process invoked for isotopic smoothing in the ice. After snow deposition, diffusion gradually affects isotopes profiles by removing the highest frequency variations, first during

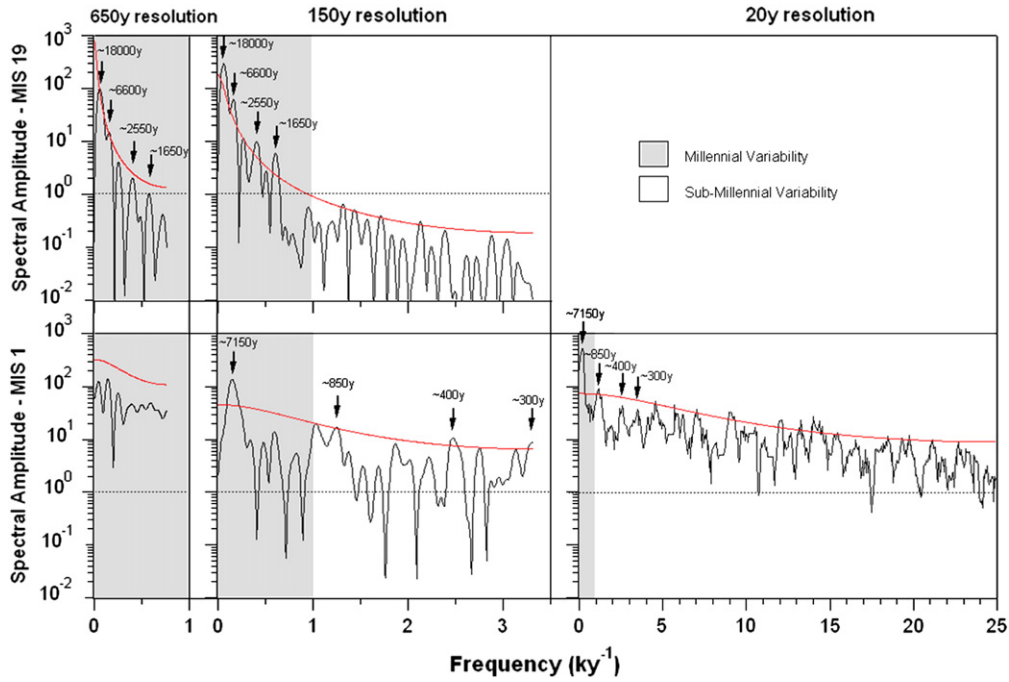


**Fig. 5.** Spectral analysis of EDC isotope data for the past first 12 ky (bottom) and from 776 to 788 ky for MIS 19 interval (top, intervals corresponding to the grey shadow areas of Fig. 2) using a Multi Taper Method (MTM, Spectra software, Ghil et al., 2002). The spectral amplitude is displayed as a function of the frequencies (in  $\text{ky}^{-1}$ ). The red lines delimit the 95% confidence interval estimated from a red noise spectrum and the grey areas delimitate millennial from sub-millennial variability. The low resolution data available for MIS 19 are re-sampled on a time step of 650 years. The high resolution data are re-sampled every 150 years. For comparison Holocene available data (with an initial resolution of  $\sim 20\text{y}$ ) have been re-sampled on the same time-steps of 650 and 150 years. The power spectrum of high resolution (20 years) Holocene data is also displayed. The periodicities of interest for the discussion are indicated with vertical arrows and labelled.

the firnification (Neumann and Waddington, 2004) and then in the solid ice (Ramseier, 1967). In the upper part of the firn, this impairment of climatic signal is due to direct exchanges between snow water molecules and vapour, involving processes such as successive change of phases (sublimation/condensation). In solid ice, self-diffusion in ice single crystals, controlled by the temperature-dependent molecular diffusivity of water stable isotopes, comes in addition to the thinning to increase the smoothing of the remaining isotope signal. Isotopic diffusion has extensively been studied and models are available for predicting the smoothing of an initial stable isotope profile for a given ice core.

Considering the classical diffusion as described in the previous short introduction, we use the methodology described in Johnsen et al. (2000) and applied for the EDC core. Based on the tracking of a layer from the surface to its actual position in the ice sheet, it requires the estimate of two parameters: (1) the vertical strain rate  $\dot{\epsilon}_z(t)$  and (2) the diffusivity of HDO molecules  $\Omega(t)$ , where  $t$  is the age and  $z$  the depth. Age is estimated as a function of depth thanks to the Dansgaard–Johnsen kink model (Johnsen and Dansgaard, 1992) modified for bottom melting and dynamic accumulation rates according the characteristics of the EDC site (Table 2). A new parameter, the diffusion length  $\sigma$ , is introduced to

describe the diffusion and its effects. It expresses the characteristic length affected by the isotopic smoothing at a given depth and is determined using the following equation:

$$\frac{d\sigma^2}{dt} - 2 \cdot \dot{\epsilon}_z(t) \cdot \sigma^2 = 2 \cdot \Omega(t), \quad (1)$$

which attributes the ice diffusion to the thinning of ice layers in the ice sheet due to the vertical strain rate and to the diffusivity of stable isotopes within the ice. The solution of Eq. (1) can be expressed as:

$$\sigma^2(t) = \sigma_{ice}^2(t) + \sigma_{firm}^2(t) \quad (2)$$

where

$$\sigma_{ice}^2(t) = \exp\left(2 \cdot \int_0^t \dot{\epsilon}_z(t') \cdot dt'\right) \left( \int_0^t 2 \cdot \Omega(t') \cdot \exp\left(\int_0^{t'} -2 \cdot \dot{\epsilon}_z(t'') \cdot dt''\right) \cdot dt' \right) \quad (3)$$

represents the diffusion occurring in the solid ice,

$$\text{and } \sigma_{firm}^2(t) = \exp\left(2 \cdot \int_0^t \dot{\epsilon}_z(t') \cdot dt'\right) \cdot \sigma_{f_0}^2 \quad (4)$$

**Table 2**  
Designation of the parameters implemented in the flow/age/thinning model (Johnsen and Dansgaard, 1992) and in the temperature/diffusion model (Johnsen et al., 1995; Johnsen et al., 2000) applied to the EPICA Dome C site.

Parameters for the flow/age/thinning model	Values or expression	Parameters for the temperature/diffusion model	Values or expression
Ice thickness	3275 (m)	Isotope-temperature slope adjusted to the LGM	$\alpha$ ( $^{\circ}\text{C}/\text{‰}$ )
Kink height	1500 (m)	temperature or best fit to the measured borehole data	$-57.0 + \alpha \times (\delta_D - \delta_0)$ ( $^{\circ}\text{C}$ )
Present deuterium value	$\delta_0 = -396.5$ (‰)	Surface temperatures	
Present accumulation rate	$ac = 0.03$ (m/y)		
Bottom melting	$0.0006$ (m/y)		
Bottom sliding factor	0.13		
Bag values corrected by sea-water isotope values	$\delta_D$ (‰)		
Past accumulation rate	$ac \times \exp((\delta_D - \delta_0) / 70.0)$ (m)		

the diffusion in the firn, with  $\sigma_{f_0}$  depending on the past temperature and accumulation rate of a given period. At the depth of MIS 19, the model shows that the isotopic diffusion occurring in the firn is negligible in front of the ice diffusion.

Here the establishment of the time scale and the estimate of the strain rate  $\dot{\epsilon}_z(t)$  represent the first sources of uncertainty for the diffusion length calculation. The thinning function (ratio of the thickness of a given layer at its present depth in the ice and its thickness when it was at the surface), is given by the first part of Eqs. (3) and (4):  $\exp\left(\int_0^t \dot{\epsilon}_z(t') \cdot dt'\right)$ . The coupled deformation and diffusion models used here (Johnsen and Dansgaard, 1992, applied to the EDC site) estimate a thinning function of  $\sim 0.035$  for MIS 19. This calculation is consistent with the independent initial estimate of Parrenin et al. (2007b) (Fig. 6a) for the establishment of the EDC3 chronology. A second source of uncertainty lies in the estimate of the deuterium molecular diffusivity  $\Omega(t)$  based on Ramseier formula (Ramseier, 1967) which depends on temperature. Fig. 6b displays two calculations of the diffusion length associated to two different in situ temperature profiles for the EDC core: the first one derived from a temperature ice flow model coupled to the diffusion model (Johnsen et al., 1995, see Table 2), and the second one forced to fit the temperature profile measured in the EDC borehole (Fig. 6c). These two profiles differ by at most 2 °C. While the results show differences between 400 and 2100 m depths, the two modelled diffusion lengths reach a common value of  $\sim 16$  cm at the depth of MIS 19 (Fig. 6b).

#### 4.4. Comparison between modelled and data-derived diffusion length

We now consider the diffusion length modelled all along the EPICA Dome C ice core consistent with the borehole temperature data. Fig. 6b



**Fig. 6.** a) Depth profiles of the thinning function from two glaciological models: EDC3 (Dreyfus et al., 2007) in green and Johnsen et al. (2000) in dark green; b) diffusion lengths calculated using the Johnsen thinning function (cm); using either the temperature profile derived from the model (light purple) or with the temperature profile fitted to the measured borehole temperatures (dark purple); c) running average over 5 m of the borehole temperature data (°C, pink) (measured in Nov 2008, offset of 5 °C for readability) and the two previously mentioned temperature profiles used for diffusion length calculation (red, model; brown, model tuned to the temperatures data); d) mean grain radius in mm (Durand et al., 2009); e)  $\delta D$  (‰) of EDC low resolution samples. The MIS19 interval is highlighted with a grey shading.

shows the slow decrease of the diffusion length with depth, from  $\sim 5$  cm near the surface to a minimum value of  $\sim 1.6$  cm at  $\sim 1900$  m, driven by the vertical thinning which progressively reduces the annual layer thickness. Near bedrock, warmer temperatures ( $> -30$  °C) enhance molecular diffusivity in the ice which results in a change of slope of the modelled diffusion length with respect to depth. The modelled diffusion length therefore increases downwards of 1900 m and reaches the previously mentioned maximum value of 16 cm in the deepest part of the core, where MIS 19 is located.

This theoretical value can be compared to the one that can be estimated from the high resolution deuterium data. The loss of high frequency variability thus revealed (see section 4.2) can be also viewed as a loss of spectral amplitude with respect to depth (cycles/m). The power spectrum associated to the data can be fitted to different power spectra of red noise that simulate different values of diffusion lengths, according to the equation  $A = A_0 \cdot \exp(-\frac{1}{2}\sigma^2 \cdot k^2)$ . This equation links the amplitude of a given harmonic cycle  $A$  recorded in the data and altered by the diffusion within the ice, to the initial amplitude  $A_0$  (with  $\sigma$  the diffusion length and  $k$  the wave number associated to the harmonic cycle); the methodology is described in Johnsen et al. (2000). This method allows us to derive an empirical diffusion length for MIS 19. The loss of spectral amplitude below  $\sim 1600$  y of periodicity discussed in Section 4.2 can thus be translated as a diffusion length estimated to reach at least 40 cm (values ranging between 40 and 60 cm depending on the fit between the corresponding red noise and the data power spectrum), a value more than twice higher than the predicted one. The strong smoothing of the deuterium signal at MIS 19 depth has therefore to be attributed to an enhanced isotopic diffusion, which cannot be simply represented by the usual processes occurring in firn and solid ice and implemented here in the Johnsen et al. (2000) classical diffusion model, which fails here to calculate the real diffusion length at the MIS 19 depth. Particular strong diffusion (or excess diffusion as called in Johnsen et al., 2000) in basal conditions has already been observed in Greenland ice cores (Johnsen et al., 1997) and models implementing new processes (Nye, 1998; Rempel and Wettlaufer, 2003a) are available. These processes are discussed in the next section.

#### 4.5. Discussion

We now explore the deep ice characteristics in cause for the observable enhanced diffusion. Fig. 6d shows the depth-profile of the grain size of ice crystals, which provide information on the ice structure. The measurements of the mean radius ( $R$ , from Durand et al., 2009) of ice crystals are displayed until 3133 m. Deeper, in the very bottom part of the core, each analysed sample displays only few grains (making difficult the measurements and increasing also the uncertainty) with high  $R$  values ( $> 10$  mm). At the same time, the EDC borehole temperatures (Fig. 6c) increase up to  $\sim -6$  °C at the depth of MIS 19 ice. A direct link can be established between the increasing grain growth observed at these depths and ice temperatures (Durand et al., 2009). The increasing grain size can indeed be attributed to migration–recrystallization processes which extend grain boundaries and are expected to take place at temperatures above  $-10$  °C (Duval and Castelnau, 1995). Such processes can contribute to the impairment of the isotopic signal by first mixing the climatic information contained in close ice crystals. In a second step, the isotopic smoothing can be enhanced by the presence of liquid water-veins within the ice (Nye, 1992). The formation of a continuous network at grain junctions is favoured when ice crystals become large, making possible the circulation of unfrozen water in the ice matrix and accelerating the diffusion of isotopes (Nye, 1998). Raisbeck et al. (2006) highlighted the presence of  $^{10}\text{Be}$  spikes deeper than  $\sim 3100$  m in the EDC core which could not be explained by production variations. As they suggested, specific horizontal concentration processes at play in the EDC deepest ice could provide an explanation for these spikes and also for the dust aggregates revealed by Lambert et al. (2008). This explanation supports our water-veins

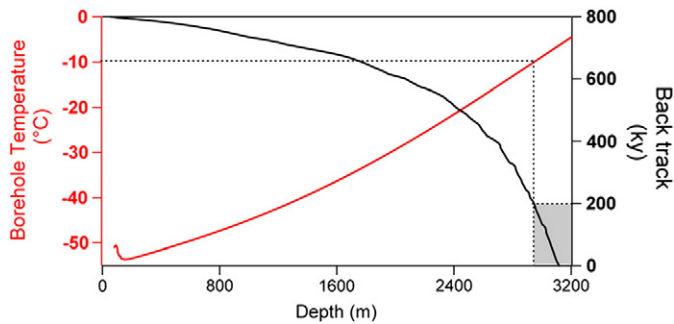


**Fig. 7.** Backtracking ice flow calculation for sample #5783 dated around 787 ky BP (expressed in ky as a function of depth, black) compared to Dome C borehole temperature profile (in °C, red). The grey area emphasizes the time spent by the ice particle at a temperature above  $-10^{\circ}\text{C}$ .

hypothesis, which is also valuable regarding the particular profiles of the MIS 19 soluble ions (ammonium and sodium) data, contrasting with the calcium (partly insoluble) profile (Fig. 4). However the behaviour of impurities in ice is still complicated to describe and interpret in such conditions (Rempel and Wettlaufer, 2003b).

The enhanced diffusion in liquid water phase has already been studied and models have been developed for its prediction (Nye, 1998; Johnsen et al., 2000 for the excess diffusion part; Rempel and Wettlaufer, 2003a). In particular, the Rempel and Wettlaufer (2003a) model taking into account the two hypotheses of the Nye and Johnsen models in their diffusion simulations can predict the excess diffusion. But quantitative calculations have not yet been performed for EDC, due to large uncertainties in the grain size estimate in the deepest part of the EDC core, which is essential to evaluate the amount of liquid water involved and to drive such diffusion model.

Using an ice flow modelling (Parrenin et al., 2007b), we can finally track an ice particle from its formation after firnification to its present location in the ice sheet. Fig. 7 shows the backtracking applied to a LR sample located at  $\sim 3163$  m. Assuming that the actual temperature profile measured in the borehole has remained unchanged in the past, we can determine when a particle had reached a given temperature. We estimate that MIS 19 ice had spent around 200ky at a temperature higher than  $-10^{\circ}\text{C}$ . We suggest that this long period, spent by the deepest ice in conditions favourable to an increased diffusion through water-veins, is responsible for the strong smoothing of climate variability (1) in stable isotopes, resulting in an apparent diffusion length reaching  $\sim 40$  cm, and (2) in the soluble ions (ammonium and sodium). The variability preserved in the calcium record is likely related to insoluble dust particles.

## 5. Conclusion and perspectives

MIS 19 occurring around 780 ky BP appears as a close “orbital analogue” for the Holocene, with orbital context more similar than during MIS 5 or MIS 11 (a point also evoked by Tzedakis, 2009). In order to improve the available temporal resolution of water stable isotope data, we have conducted new deuterium measurements on 395 high resolution samples for the period between MIS 20 and MIS 18. Despite the improved resolution from  $\sim 650$  y to  $\sim 130$  y confirming earlier results, no new information on MIS 19 climate variability has been revealed, because of a strong smoothing of the deuterium signal. This smoothing, highlighted by a loss of spectral amplitude below a periodicity of  $\sim 1600$  y, contrasts with the sub-millennial variability preserved for Holocene at comparable resolution and in MIS 19 high resolution calcium data. The spectral analysis thus reveals an enhanced isotopic diffusion, occurring in the deepest ice of EDC core. We have shown that the predictions of the Johnsen et al. (2000) classical model, considering the classical diffusion occurring both in the firn and the solid

ice, under-estimates the observed MIS 19 diffusion length estimated from our data, by at least a factor of two.

To explain our result, we have investigated other EDC records and physical processes at play in the very bottom part of the core. High values of ice grain size (Durand et al., 2009) and warm temperatures in the borehole ( $\sim -6^{\circ}\text{C}$ ) measured at MIS 19 location depths, suggests the presence of water-veins at the grain junctions. This is also supported by strongly smoothed records of soluble ions (ammonium and sodium). A continuous liquid water network is expected to strongly enhance isotopic diffusion compared to the “classical diffusion” in the solid ice (Nye, 1998). In addition we have estimated the time period spent by the MIS 19 old ice at temperatures warmer than the critical value of  $-10^{\circ}\text{C}$ , expected to be a threshold for migration–recrystallization processes (Duval and Castelnau, 1995). Our results suggest that ice stored for 200 ky above  $-10^{\circ}\text{C}$  undergoes extra diffusion processes which double the diffusion length.

The lack of new information on sub-millennial climate variability during MIS 19 is frustrating because it prevents any further high frequency comparison with previous interglacials (with the exception of calcium). Even though we are limited by large uncertainties on ice grain size in the deepest part of the EDC core, sensitivity tests could be performed with the Rempel and Wettlaufer model (2003a) to depict the evolution of diffusion length prior to the MIS 19 depth and to determine the progressive erasing of high frequency climate variability in deep EDC ice. High resolution data prior to MIS 19 could also provide valuable datasets for model–data comparisons, allowing to quantify the importance of water-veins in deep ice. Such information could as well be useful for the dielectric properties of deep ice and the interpretation of radar data (Carter et al., 2009; Wolff et al., 2010b).

The knowledge of possible mechanisms at play in the deepest part of the ice sheets that are able to erase high frequency climate variability is important in the perspective of future challenges, such as the “oldest ice challenge” (<http://www.pages-igbp.org/ipics/>). A proper preservation of this variability prior to one thousand kilo-years requires the selection of a deep drilling site with low accumulation and deepest ice temperatures as cold as possible.

## Acknowledgements

The authors wish to thank in particular R. Röthlisberger and E. Wolff for the data communication and help and G. Raisbeck for the helpful discussion. They are very grateful to the two anonymous reviewers who have contributed to improve the manuscript. This work is a contribution to the European Project for Ice coring in Antarctica (EPICA), a joint European Science Foundation/European Commission (EU) scientific program, funded by the EU and by national contributions from Belgium, Denmark, France, Germany, Italy, The Netherlands, Norway, Sweden, Switzerland and the U.K. This work has in particular benefited from the support of EPICA-MIS, ANR PICC and ANR Dome A. This is EPICA publication n°270 and LSCE publication n°4398.

## References

- Berger, A., Loutre, M.F., 1991. Insolation values for the climate of the last 10 million years. *Quaternary Sciences Reviews* 10, 297–317.
- Bigler, M., Röthlisberger, R., Lambert, F., Wolff, E.W., Castellano, E., Udisti, R., Stocker, T.F., Fischer, H., 2010. Atmospheric decadal variability from high-resolution Dome C ice core records of aerosol constituents beyond the Last Interglacial. *Quaternary Science Reviews* 29, 324–337.
- Bintanja, R., van de Wal, R., Oerlemans, J., 2005. Modelled atmospheric temperatures and global sea levels over the past million years. *Nature* 437, 125–128.
- Carter, S.P., Blankenship, D.D., Young, D.A., Holt, J.W., 2009. Using radar-sounding data to identify the distribution and sources of subglacial water: application to Dome C, East Antarctica. *Journal of Glaciology* 55, 1025–1040.
- Dreyfus, G., Parrenin, F., Lemieux-Dudon, B., Durand, G., Masson-Delmotte, V., Jouzel, J., Barnola, J.M., Panno, L., Spahni, R., Tisserand, A., Siegenthaler, U., Leuenberger, M., 2007. Anomalous flow below 2700 m in the EPICA Dome C ice core detected using  $\delta^{18}\text{O}$  of atmospheric oxygen measurements. *Climate of the Past* 3, 341–353.

- Dreyfus, G.B., Raisbeck, G.M., Parrenin, F., Jouzel, J., Guyodo, Y., Nomade, S., Mazaud, A., 2008. An ice core perspective on the age of the Matuyama–Brunhes boundary. *Earth and Planetary Science Letters* 274, 151–156.
- Durand, G., Svensson, A., Persson, A., Gagliardini, O., Gillet-Chaulet, F., Sjolte, J., Montagnat, M., Dahl-Jensen, D., 2009. Evolution of the texture along the EPICA Dome C ice core. *Physics of ice core records II* 68, 91–105.
- Duval, P., Castelnau, O., 1995. Dynamic recrystallization of ice in polar ice sheets. *Journal de Physique* 5, 197–206.
- EPICA-community-members, 2004. Eight glacial cycles from an Antarctic ice core. *Nature* 429, 623–628.
- EPICA-community-members, 2006. One-to-one coupling of glacial climate variability in Greenland and Antarctica. *Nature* 444, 195–198.
- Ghil, M., Allen, M.R., Dettinger, M.D., Ide, K., Kondrashov, D., Mann, M., Robertson, A.W., Tian, Y., Varadi, F., You, P., 2002. Advanced spectral methods for climatic time series. *Reviews of Geophysics* 40, 1–41.
- Johnsen, S.J., Dansgaard, W., 1992. On flow model dating of stable isotope records from Greenland ice cores. In: Bard, E., Broecker, W.S. (Eds.), *The Last Deglaciation: Absolute and Radiocarbon Chronologies*. Springer-Verlag, New-York, pp. 13–24.
- Johnsen, S.J., Dahl-Jensen, D., Dansgaard, W., Gundestrup, N., 1995. Greenland paleotemperatures derived from GRIP bore hole temperature and ice core isotope profiles. *Tellus* 47B, 624–629.
- Johnsen, S.J., Clausen, H.B., Dansgaard, W., Gundestrup, N.S., Hammer, C.U., Andersen, U., Andersen, K.K., Hvidberg, C.S., Dahl-Jensen, D., Steffensen, J.P., Shoji, H., Sveinbjörnsdóttir, A.E., White, J.W.C., Jouzel, J., Fisher, D., 1997. The  $\delta^{18}\text{O}$  record along the Greenland Ice Core Project deep ice core and the problem of possible Eemian climatic instability. *Journal of Geophysical Research* 102, 26397–26410.
- Johnsen, S.J., Clausen, H.B., Cuffey, K.M., Hoffmann, G., Schwander, J., Creyts, T., 2000. Diffusion of stable isotopes in polar firn and ice: the isotope effect in firn diffusion. In: Hondoh, T. (Ed.), *Physics of Ice Core Records*. Hokkaido University Press, Sapporo, pp. 121–140.
- Jouzel, J., Vaikmae, R., Petit, J.-R., Martin, M., Duclos, Y., Stievenard, M., Lorius, C., Toots, M., Mélières, M.-A., Burckle, L.H., Barkov, N.I., Kotlyakov, V.M., 1995. The two-step shape and timing of the last deglaciation in Antarctica. *Climate Dynamics* 11, 151–161.
- Jouzel, J., Masson, V., Cattani, O., Falourd, S., Stievenard, M., Stenni, B., Longinelli, A., Johnsen, S.J., Steffensen, J.P., Petit, J.R., Schwander, J., Souchez, R., Barkov, N.I., 2001. A new 27 ky high resolution East Antarctic climate record. *Geophysical Research Letters* 28, 3199–3202.
- Jouzel, J., Masson-Delmotte, V., Cattani, O., Dreyfus, G., Falourd, S., Hoffmann, G., Minster, B., Nouet, J., Barnola, J.M., Chappellaz, J., Fischer, H., Gallet, J.C., Johnsen, S., Leuenberger, M., Loulergue, L., Luthi, D., Oerter, H., Parrenin, F., Raisbeck, G., Raynaud, D., Schilt, A., Schwander, J., Selmo, E., Souchez, R., Spahni, R., Stauffer, B., Steffensen, J.P., Stenni, B.S., 2007. T.F., Tison, J.L., Werner, M., Wolff, E., Orbital and millennial Antarctic climate variability over the past 800,000 years. *Science* 317, 793–796.
- Lambert, F., Delmonte, B., Petit, J.R., Bigler, M., Kaufman, P.R., Hutterli, M., Stocker, T.F., Ruth, U., Steffensen, J.P., Maggi, V., 2008. Dust-climate couplings over the past 800,000 years from the EPICA Dome C ice core. *Nature* 452, 616–619.
- Laskar, J., Joutel, F., Boudin, F., 1993. Orbital, precessional, and insolation quantities for the Earth from –20Myr to +10Myr. *Astronomy and Astrophysics* 270, 522–533.
- Loulergue, L., Schilt, A., Spahni, R., Masson-Delmotte, V., Blunier, T., Lemieux, B., Barnola, J.M., Raynaud, D., Stocker, T., Chappellaz, J., 2008. Orbital and millennial-scale features of atmospheric  $\text{CH}_4$  over the last 800,000 years. *Nature* 453, 383–386.
- Loutre, M.F., 2003. Clues from MIS 11 to predict the future climate – a modelling point of view. *Earth and Planetary Science Letters* 212, 213–224.
- Loutre, M.F., Berger, A., 2003. Marine Isotope Stage 11 as an analogue for the present interglacial. *Global and Planetary Change* 36, 209–217.
- Lüthi, D., Floch, M.L., Bereiter, B., Blunier, T., Barnola, J.M., Siegenthaler, U., Raynaud, D., Jouzel, J., Fischer, H., Kawamura, K., Stocker, T.F., 2008. High resolution carbon dioxide concentration record 650,000–800,000 years before present. *Nature* 453, 379–382.
- Masson, V., Vimeux, F., Jouzel, J., Morgan, V., Delmotte, M., Ciais, P., Hammer, C., Johnsen, S., Lipenkov, V.Y., Mosley-Thompson, E., Petit, J.-R., Steig, E., Stievenard, M., Vaikmae, R., 2000. Holocene climate variability in Antarctica based on 11 ice cores isotopic records. *Quaternary Research* 54, 348–358.
- Masson-Delmotte, V., Stenni, B., Jouzel, J., 2004. Common millennial scale variability of Antarctic and Southern Ocean temperatures during the past 5000 years reconstructed from EPICA Dome C ice core. *Holocene* 14, 145–151.
- Masson-Delmotte, V., Dreyfus, G., Braconnot, P., Johnsen, S., Jouzel, J., Kageyama, M., Landais, A., Loutre, M.F., Nouet, J., Parrenin, F., Raynaud, D., Stenni, B., Tuenter, E., 2006. Past temperature reconstructions from deep ice cores: relevance for future climate change. *Climate of the Past* 2, 145–165.
- Masson-Delmotte, V., Stenni, B., Pol, K., Braconnot, P., Cattani, O., Falourd, S., Kageyama, M., Jouzel, J., Landais, A., Minster, B., Barnola, J.M., Chappellaz, J., Kriener, G., Johnsen, S., Röthlisberger, R., Hansen, J., Mikolajewicz, U., Otto-Blieneser, B., 2010. EPICA Dome C record of glacial and interglacial intensities. *Quaternary Science Reviews* 29, 113–128.
- Monnin, E., Indermühle, A., Dällenbach, A., Flückiger, J., Stauffer, B., Stocker, T., Raynaud, D., Barnola, J.M., 2001. Atmospheric  $\text{CO}_2$  concentrations over the last glacial termination from the Dome Concordia, Antarctica, ice core. *Science* 291, 112–114.
- Neumann, T.A., Waddington, E.D., 2004. Effects of firn ventilation on isotopic exchange. *Journal of Glaciology* 169, 183–194.
- Nye, J.F., 1992. Water veins and lenses in polycrystalline ice. *Physics and Chemistry of Ice*. In: Maeno, N., Hondoh, T. (Eds.), Hokkaido University Press, Sapporo, pp. 200–206.
- Nye, J.F., 1998. Diffusion of isotopes in the annual layers of ice sheets. *Journal of Glaciology* 44, 467–468.
- Paillard, D., 1998. The timing of Pleistocene glaciations from a simple multiple-state climate model. *Nature* 391, 378–381.
- Parrenin, F., Barnola, J.M., Beer, J., Blunier, T., Castellano, E., Chappellaz, J., Dreyfus, G., Fischer, H., Fujita, S., Jouzel, J., Kawamura, K., Lemieux-Dudon, B., Loulergue, L., Masson-Delmotte, V., Narcisi, B., Petit, J.R., Raisbeck, G., Raynaud, D., Ruth, U., Schwander, J., Severi, M., Spahni, R., Steffensen, J.P., Svensson, A.M., Udisti, R., Waelbroeck, C., Wolff, E., 2007a. The EDC3 chronology for the EPICA Dome C ice core. *Climate of the Past* 3, 485–497.
- Parrenin, F., Dreyfus, G., Durand, G., Fujita, S., Gagliardini, O., Gillet, F., Jouzel, J., Kawamura, K., Lhomme, N., Masson-Delmotte, V., Ritz, C., Schwander, J., Shoji, H., Uemura, R., Yoshida, N., Watanabe, O., Wolff, E.W., 2007b. Ice flow modelling at Dome C and Dome Fuji, East Antarctica. *Climate of the Past* 3, 243–259.
- Pollard, D., DeConto, R.M., 2009. Modelling West Antarctic ice sheet growth and collapse through the past five million years. *Nature* 458, U329–U389.
- Raisbeck, G.M., You, F., Cattani, O., Jouzel, J., 2006. Be-10 evidence for the Matuyama–Brunhes geomagnetic reversal in the EPICA Dome C ice core. *Nature* 444, 82–84.
- Ramseier, R.O., 1967. Self-diffusion of tritium in natural and synthetic ice monocrystals. *Journal of Applied Physics* 38, 2553–2556.
- Rempel, A.W., Wettlaufer, J.S., 2003a. Isotopic diffusion in polycrystalline ice. *Journal of Glaciology* 49, 397–406.
- Rempel, A.W., Wettlaufer, J.S., 2003b. Segregation, transport, and interaction of climate proxies in polycrystalline ice. *Canadian Journal of Physics* 81, 89–97.
- Ruddimann, W., 2005. Cold climate during the closest stage 11 analog to recent millennia. *Quaternary Science Reviews* 24, 1111–1121.
- Siengenthaler, U., Stocker, T.F., Monnin, E., Lüthi, D., Schwander, J., Stauffer, B., Raynaud, D., Barnola, J.-M., Fischer, H., Masson-Delmotte, V., Jouzel, J., 2005. Stable carbon cycle–climate relationship during the last Pleistocene. *Science* 310, 1313–1317.
- Spahni, R., Chappellaz, J., Stocker, T.F., Loulergue, L., Hausammann, G., Kawamura, K., Flückiger, J., Schwander, J., Raynaud, D., Masson-Delmotte, V., Jouzel, J., 2005. Variations of atmospheric methane and nitrous oxide during the last 650,000 years from Antarctic ice cores. *Science* 310, 1317–1321.
- Tzedakis, P.C., 2009. The MIS 11–MIS 1 analogy, southern European vegetation, atmospheric methane and the “early anthropogenic hypothesis”. *Climate of the Past Discussion* 5, 1337.
- Vaughn, B., White, J.W.C., Delmotte, M., Trolier, M., Cattani, O., Stievenard, M., 1998. An automated system for the uranium reduction method of hydrogen isotope analysis of water. *Chemical Geology* 152, 309–319.
- Wolff, E.W., Barbante, C., Becagli, S., Bigler, M., Boutron, C.F., Castellano, E., de Angelis, M., Federer, U., Fischer, H., Fundel, F., Hansson, M., Hutterli, M., Jonsell, U., Karlin, T., Kaufmann, P., Lambert, F., Littot, G.C., Mulvaney, R., Röthlisberger, R., Ruth, U., Severi, M., Siggaard-Andersen, M.L., Sime, L.C., Steffensen, J.P., Stocker, T.F., Traversi, R., Twarloh, B., Udisti, R., Wagenbach, D., Wegner, A., 2010a. Changes in environment over the last 800,000 years from chemical analysis of the EPICA Dome C ice core. *Quaternary Science Reviews* 29, 285–295.
- Wolff, E.W., Fischer, H., Wilhelm, F., 2010b. Chemical Control on Electrical Records from Central Antarctic Ice Cores. *International Polar Year—Oslo Science Conference, Oslo—Norway*.
- Yiou, P., Fuhrer, K., Meeker, L.D., Jouzel, J., Johnsen, S., Mayewski, P.A., 1997. Paleoclimatic variability inferred from the spectral analysis of Greenland and Antarctic ice core data. *Journal of Geophysical Research* 102, 26441–26454.